Eur. Phys. J. D **38**, 103–109 (2006)
DOI: 10.1140/epjd/e2006-00030-6

THE EUROPEAN PHYSICAL JOURNAL D

Energy transfer in hyperthermal Xe-graphite surface scattering

Y. Watanabe[1,a], H. Yamaguchi[2], M. Hashinokuchi[1], K. Sawabe[1], S. Maruyama[2], Y. Matsumoto[2], and K. Shobatake[1,3]

[1] Graduate School of Engineering, Nagoya University, Furo-cho, Chikusa-ku, Nagoya 464-8603, Japan
[2] Department of Mechanical Engineering, The University of Tokyo, 7-3-1 Hongo Bunkyo-ku, Tokyo 113-8656, Japan
[3] Toyota Physical & Chemical Research Institute, Nagakute, Aichi 480-1192, Japan

Received 4 November 2005 / Received in final form 12 December 2005
Published online 8 February 2006

Abstract. The scattering of a hyperthermal Xe from a graphite (0001) surface has been studied using a molecular beam-surface scattering technique and molecular dynamics (MD) simulations. The angular and velocity distributions of scattered Xe atoms were measured at incidence energies from 0.45 to 3.5 eV, three incidence angles of 15°, 35° and 60° and the surface temperatures of 300 K and 550 K. The observed time-of-flight spectra exhibit a sharp velocity distribution with only one velocity component, which is ascribed to the direct inelastic scattering process. The angle-resolved energy ratios of the mean final translational energy over the mean incidence energy E_f/E_i agree well with those predicted based on the assumption of the conservation of the momentum parallel to the surface. The Hard-Cube model, where the mass of the cube is approximately 310 u, has reproduced the angle-resolved flux distributions of scattered Xe atoms. In the Hard-Cube model almost 80% of the normal component of the incidence translational energy is found to be lost in collision. The MD simulations reproduce well the experimental results by using the Brenner potential for intralayer C atoms and a Lennard-Jones potential for interlayer C–C pair interactions.

PACS. 68.49.Bc Atom scattering from surfaces (diffraction and energy transfer) – 68.49.Df Molecule scattering from surfaces (energy transfer, resonances, trapping)

1 Introduction

Molecular beam-surface scattering is an effective technique for understanding the fundamental processes of gas-surface energy exchange in collision and clarifying a gas-surface potential [1–3]. Information on the energy transfer from an incident gas molecule to a surface is needed for modeling of many chemical or physical phenomena. Knowledge of the interaction potential of the system is valuable for predicting surface phenomena and reactions, for example trapping and sticking of molecules at low energies [4,5], and the sputtering and etching at high energies [6,7]. The dynamics and energy transfer in collision of a gas molecule with a surface, however, are complicated since they depend on the experimental conditions such as the translational energy and the angle of an incident projectile, a gas/surface mass ratio, the surface temperature, and the gas-surface potential energy surface all contribute.

A lot of gas-surface collision experiments have been performed and several simplifications have been presented to model the dynamics and the energy transfers. At relatively low incidence energies the energy transfer process is explained in terms of the binary collision between a hard sphere and a cube [8–10]. The model is recognized as a "Hard-Cube model". It rests on the assumption that the tangential component of momentum of the atom is conserved during collision with the flat surface. The perpendicular component of the momentum is altered via an impulsive hard wall collision with a vibrating surface cube. Even though the Hard-Cube model is simple, it has been remarkably successful in explaining experimental results in the thermal incidence translational energy range, especially in the cases of a light gas atom impact upon a heavy surface atom [11,12].

Dynamics of a gas-surface scattering are strongly influenced by the gas-surface potential energy hypersurface. At hyperthermal incidence energies an incident particle penetrates deeply into the repulsive part of the interaction potential and feels a corrugation inherent to the surface structure [11–13]. A "Washboard model" describes the dynamics of scattering from a highly corrugated surface [14]. The corrugation in the gas-surface potential is static and dynamic by nature. An atomically corrugated surface potential, which is derived from the surface lattice structure [13,14] or adsorbates covered on surface, leads to a statically corrugated gas-surface potential [15,16]. Under such circumstances, the incidence parallel and perpendicular momenta to the surface are changed in collision.

[a] e-mail: h036604d@mbox.nagoya-u.ac.jp

Dynamic corrugation in a gas-surface potential is generated when the surface is deformed by the collision with the incident molecule [17,18]. In the case that the incident particle mass is much greater than that of surface atom, e.g., Xe/Ni [17], the dynamic corrugation in the gas-surface potential is induced, though in a Xe/Pt system [19] there is no evidence for such corrugation. When the dynamic corrugation is induced by the deformation of the surface in collision, the presence of many atoms at a surface would help dissipate the collision energy through lattice phonon and the energy transfer process becomes more complicated. The understanding of the complex dynamics of the collision process is expected to be greatly improved by measuring the angular and velocity distributions of molecules scattered from a surface.

In the present article, we employ both experiments and simulations to investigate the energy transfer mechanism for collision of Xe atoms with a graphite (0001) surface. Previously we investigated the same system at thermal incidence energies $\leq$0.45 eV and discussed about the degree of energy transfer [20]. Någård et al. reported molecular beam experiments and MD simulations of Xe scattered from the graphite surface for a wide range of incidence conditions [21]. Although their MD simulations gave a good agreement with experiments at low incidence energies, deviations became prominent at higher energies. It is probably because in the experiment of Någård et al. the distance from a sample to a detector was too short to determine the reliable translational energies of the scattered atoms. There is less information available in the heavy atom hyperthermal scattering regime. In order to derive a more detailed understanding of the Xe-graphite interaction at hyperthermal incidence energies, the Xe-graphite surface scattering experiments have been conducted using an apparatus in which the flight distance from the sample surface to the ionization region in time-of-flight measurements is long enough to give accurate velocity distributions. The preliminary results have already been published elsewhere [22]. In the present article the detailed descriptions are presented.

2 Experimental and simulation methods

2.1 Experimental

The scattering experiments have been carried out on a molecular beam apparatus that has been described by Yoshikawa et al. [23]. In brief the molecule-surface scattering apparatus consists of a three-stage differentially pumped molecular beam line, an ultrahigh vacuum (UHV) chamber, and a differentially pumped quadrupole mass spectrometer (QMS) chamber. The detector chamber can be rotated in the range of the detector position Θ_p from $\Theta_p = 0°$ (which defines the direction of the incident beam) to the maximum angle of $\Theta_p = 145°$ in order to measure angular distributions of scattered particles from the surface. The relation $\Theta_p + \theta_i + \theta_f = 180°$ holds, where θ_i and θ_f are the incidence and the scattering angle, respectively, as measured from the surface normal. Thus the scattering angle, given by $\theta_f = 180° - \theta_i - \Theta_p$, spans from $\theta_f = 35° - \theta_i$ to the maximum scattering angle of 90° around the sample.

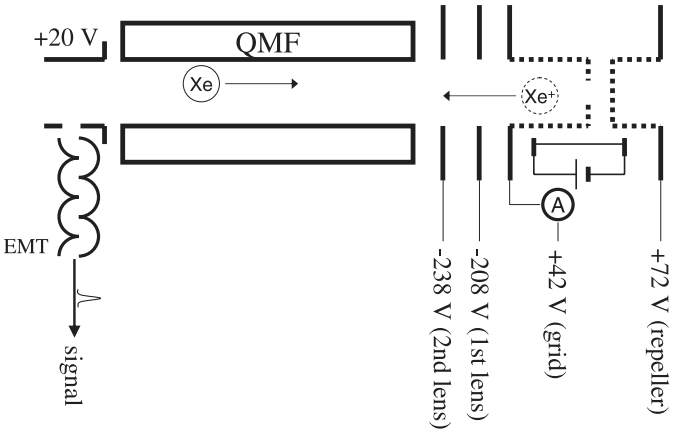

Fig. 1. Scheme of electronic block diagram for the mass spectrometer detector and modified ionlens system. The typical lens voltages are shown. The repeller lens (+72 V) was placed behind the grid to reflect the Xe ion.

We used a graphite (0001) plate (Matsushita Electric Industrial Co., Ltd). Prior to measurements, contamination of the sample was removed by annealing up to 550 K for several hours. The measurements were made at surface temperatures of $T_s = 300$ K and 550 K. A hyperthermal Xe atom beam was formed by a supersonic expansion of a gas mixture from a Pt nozzle with a diameter of 30 μm. The translational energy of the incident beam was controlled by varying the seeding ratio of Xe to He and/or the stagnation temperature. A time-of-flight (TOF) technique was employed to determine the velocity distributions of the incident and scattered atoms. The atom beam was pulsed with a rotating mechanical chopper disk placed before entering the sample camber. The flight length between the sample surface and the ionizer region is 34.7 cm, which is long enough to obtain accurate velocity distributions for particles with hyperthermal energies.

In order to elongate the flight length between the sample surface and an ionizer region, the ionizer was placed downstream of the quadrupole mass (QMS) filter. For the present study the lens system of the ionizer was modified as shown in the schematic drawing of the lens voltages in Figure 1. The main point of the modification is a placement of a repeller behind the grid. Xe atoms entering in the ionizer region from left to right are ionized by electron bombardment. The ions are extracted toward the reverse direction, mass-filtered through the QMS filter axis, deflected by 90° and detected with an electron multiplier tube (EMT).

When the repeller was not placed, we had a great difficulty in detecting atoms with hyperthermal energies. As the translational energy of the neutral particle was increased, exceeding about 1 eV, the detection efficiency went down drastically. When the ion formed in the ionizer turns and leaves from the grid, the ion energy becomes

high depending on the potential P eV at the position of ionization in the grid. The translational energy of the ions moving at the ground potential field is approximately given as $(P + E_t)$ eV when the translational energy of the entering neutral particles is E_t eV. The potential P eV at the position in the ionizer grid varies as $P = V_g - V_{space} - V_{ex}$, in which V_g is the grid voltage, V_{space} the potential drop due to the space charge of ionizing electrons, and V_{ex} the potential drop due to the contribution of the extractor lens voltage. If the sum of potential drops due to the latter two terms, $(V_{space} + V_{ex})$, is larger than E_t, the ions formed in the ionizer can be successfully repelled backward. If an entering neutral particle has a translational energy E_t higher than $(V_{space} + V_{ex})$, the ions go through the grid and will be never repelled backward.

For mass spectrometer detectors used for beam detection with a structure in which the quadrupole mass filter is placed downstream of the ionizer, the ions are extracted more or less in the same direction of the neutral beam motion and thus they can be detected efficiently. However when mass spectrometer detectors have a structure where a momentum changes drastically from a neutral beam to an ionized beam, the similar problems should arise, especially for detection of neutral species with hyperthermal translational energies. The problem has been solved by placing of a repeller behind the grid. To make sure that the Xe ions formed from incoming hyperthermal Xe atoms are extracted into the reverse direction, the 3rd lens (repeller) was biased at +72 V, i.e. by the lens which is 30 V higher than the ion grid voltage, the detection efficiency of hyperthermal Xe atoms has been dramatically improved.

2.2 Molecular dynamics simulation

The molecular dynamics method has been used to simulate the scattering of a Xe atom from a graphite surface. The trajectories of the gas atom and the surface atoms were calculated solving the Newton's equations of motions using the leap-frog method, where the time step was set at 0.5 fs [24,25].

The interaction between the Xe atom and the solid surface was represented by a sum of the site-to-site Lennard-Jones (12–6) potentials. The potential parameters ϵ and σ were set to be 9.102 meV and 3.358 Å, respectively. Six layers of 384 carbon atoms and the Miller index of the (0001) surface were taken into consideration. Periodic boundary conditions were applied to construct a wide thin film of graphite. Two model potentials were used for graphite potentials. One is the harmonic model which employs harmonic potentials (between intraplanar atoms: well depth $\epsilon = 44.44$ eV, $r_e = 1.42$ Å, between atoms in different planes: 6.39 eV, 3.40 Å) [26]. In another model a Lennard-Jones potential (12-6) was used as the interlayer site-to-site potential between carbon atoms in different planes ($\epsilon = 2.40$ meV and $\sigma = 3.37$ Å) and the Brenner potential was used for carbon atoms in the same graphite layer [27]. The latter model is quite similar to that Någård et al. have employed [21]. Before starting calculations of gas-surface collision, a thin film of graphite at thermal equilibrium of $T_s = 300$ K or 550 K was prepared. After 50,000 steps of temperature control and 50,000 steps without temperature control, the graphite surface attained a thermal equilibrium. Next, Xe atoms were allowed to collide with the graphite surface one at a time. The initial translational energy was stochastically given so a velocity distribution of the incident Xe atoms in our MD calculations agrees with that determined from the observed TOF spectrum of the molecular beam, while Någård et al. adopted one particular translational energy for the incident atoms. The simulation was continued for 100,000 steps, or until the gas atom escaped from the surface. If the total energy of the gas atom was lower than $-2kT_g$, the atom was defined as being trapped. After each collision, the solid surface was set back to the initial condition. For each incidence condition 10,000 trajectories were calculated.

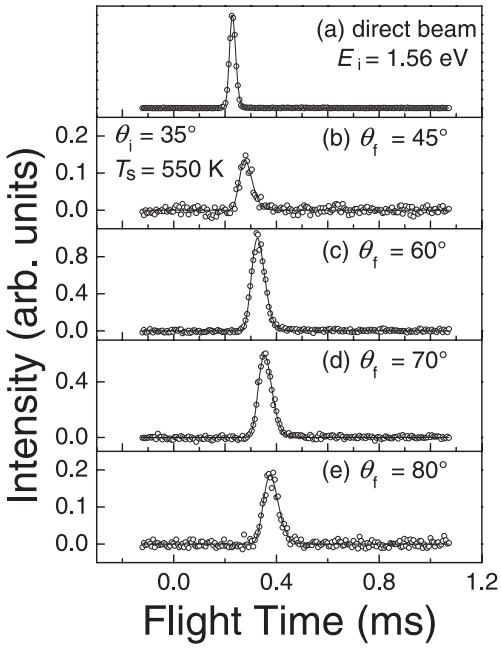

Fig. 2. TOF spectra of (a) the incident Xe beam $E_i = 1.56$ eV, and the atoms scattered from the graphite surface for $T_s = 550$ K, $\theta_f =$ (b) 45°, (c) 60°, (d) 70°, and (e) 80°.

3 Results

3.1 Xe-graphite (0001) surface scattering experiment

We have performed Xe-graphite (0001) surface scattering experiments under various incidence conditions. Angular flux distributions and velocity distributions were measured at each scattering angle as a function of incidence energy, incidence angle and surface temperature. Figure 2 shows TOF spectra of the direct beam (a) and the scattered Xe atoms detected at the scattering angles θ_f of 45° (b), 60° (c), 70° (d), and 80° (e) with respect to the

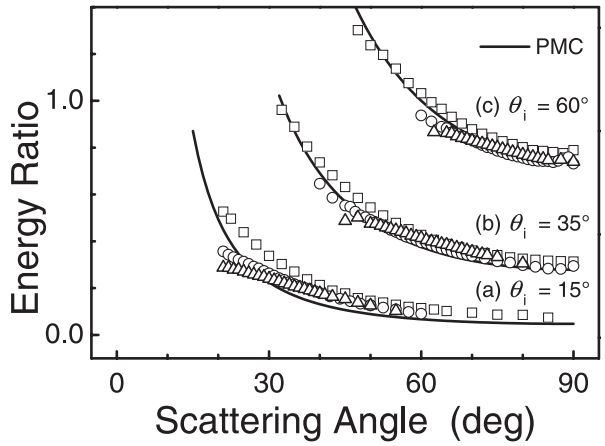

Fig. 3. Variation of the mean final energy relative to the incidence energy (E_f/E_i) for Xe atoms scattered from the graphite (0001) at T_s = 550 K for θ_i = (a) 15°, (b) 35°, and (c) 60°. The initial kinetic energies in eV are (a) 0.45 (□), 1.56 (○) and 3.29 (△); (b) 0.45 (□), 1.65 (○) and 3.62 (△); (c) 0.45 (□), 1.63 (○) and 3.49 (△). The curves are theoretical E_f/E_i ratios expected for the strict parallel momentum conservation (PMC).

surface normal. The incidence angle θ_i is 35°, the initial kinetic energy E_i is 1.65 eV, and the surface temperature T_s is 550 K. All of the TOF spectral intensities are scaled in such a way that the peak intensity at $\theta_f = 60°$ is normalized to 1.0. As shown in Figure 2a, we have observed a sharp TOF profile for the incident beam after modifying the ion lens system. The velocity distributions of the hyperthermal atom beam have been accurately determined. The scattered atom spectra in Figures 2b–2e exhibit only one velocity component almost as sharp as that of the incident beam. This component is ascribed to the scattered atoms from the direct-inelastic scattering process. All of the TOF spectra have been well fitted to only one shifted Maxwell-Boltzmann distribution.

Figure 3 shows the angle-resolved energy ratios of the mean final translational energy of the scattered atoms over the mean incidence energy E_f/E_i for $E_i \approx 0.45$, 1.5 and 3.5 eV. The surface temperature T_s is 550 K and the incidence angles θ_i are 15° (a), 35° (b) and 60° (c). The solid lines in Figure 3 are the energy ratio curves predicted from the conservation of momentum parallel to the surface; the strict parallel momentum conservation (PMC) requires that $E_f/E_i = (\sin\theta_i/\sin\theta_f)^2$ for all scattering angles. For $\theta_i = 35°$ and 60°, it is apparent that the energy ratio curves follow the prediction of PMC at not only low incidence energy but also hyperthermal incidence energies. The results are the evidence that Xe atoms are scattered from a flat surface for a wide incidence energy range. At $\theta_i = 15°$, however, the experimental results slightly deviate from the PMC prediction at small scattering angles. Någård et al. have reported that the energy ratios (in fact they estimated the average velocity) in Xe-graphite scattering appreciably deviate from the PMC predictions, especially for high incidence energies [21]. However, the energy ratios obtained from our experiments agree with the PMC predictions, even at high incidence energies. The discrepancy must be partly due to the fact that the surface-ionizer distance (4.5 cm) in their apparatus is too short to obtain accurate speed distributions, whereas in the present study the surface-ionizer distance is sufficiently long (34.7 cm).

The simple classical model for the scattering of gas atoms from a solid surface is described as a simple Hard-Cube model in which the attractive force is not taken into consideration. Since the results of the energy ratios of Xe atoms scattered from graphite (0001) surface in Figure 3 follow the prediction of PMC for all incidence conditions, the Hard-Cube model is employed to simulate the angular flux distribution of inelastically scattered Xe atoms from a smooth graphite (0001) surface. Logan and Stickney have given the angular distribution of the flux of gas atoms leaving the surface [10]. In their model, the velocity distributions for incident gas atoms and surface atoms are given by the Maxwellian distribution. We modified the equations of their model because the incident beam has single shifted Maxwell-Boltzmann distribution. Our model assumes that the incident atoms have a constant velocity u_i ($u_{i,\perp}$ is the perpendicular component of u_i) and the surface cube has a one-dimensional Maxwellian distribution for the velocity U_0 dependent on the surface temperature T_s. The perpendicular velocity axis is taken to point downward or from vacuum towards the bulk solid. The differential rate at which collisions occur between incident gas atoms and surface cube is

$$\mathrm{d}R = (u_{i,\perp} - U_0)G_0(U_0)\mathrm{d}U_0. \quad (1)$$

The probability distribution of the flux of gas atoms leaving the surface for scattering at angle θ_f is given by

$$\frac{\mathrm{d}R}{\mathrm{d}\theta_f} \propto (u_{i,\perp} - U_0)G_0(U_0)\left|\frac{\mathrm{d}U_0}{\mathrm{d}\theta_f}\right|. \quad (2)$$

The Maxwellian velocity distribution for the surface cube is

$$G_0(U_0)\mathrm{d}U_0 = \left(\frac{M}{2\pi kT_s}\right)^{\frac{1}{2}} \exp\left(\frac{-MU_0^2}{2kT_s}\right)\mathrm{d}U_0 \quad (3)$$

where M is the effective mass of the surface cube.

In Figure 4 the observed angular flux distribution estimated from the TOF spectra is compared with the best-fit theoretical flux distribution estimated from equation (2). The experimental values are denoted by open circles and the solid line is the theoretical distribution. The incidence conditions are $\theta_i = 35°$ and (a) E_i = 1.36 eV, T_s = 300 K, (b) E_i = 3.44 eV, T_s = 300 K, (c) E_i = 1.56 eV, T_s = 550 K, and (d) E_i = 3.62 eV, T_s = 550 K. The effective mass of the surface cube M in equation (3) has been determined so that the calculated angular distribution fits best to the observed one. The angular flux distributions of experimental result are well reproduced in terms of the Hard-Cube model. In the model, the width of the angular distribution is attributed to the degree of normal momentum transfer associated with different cube

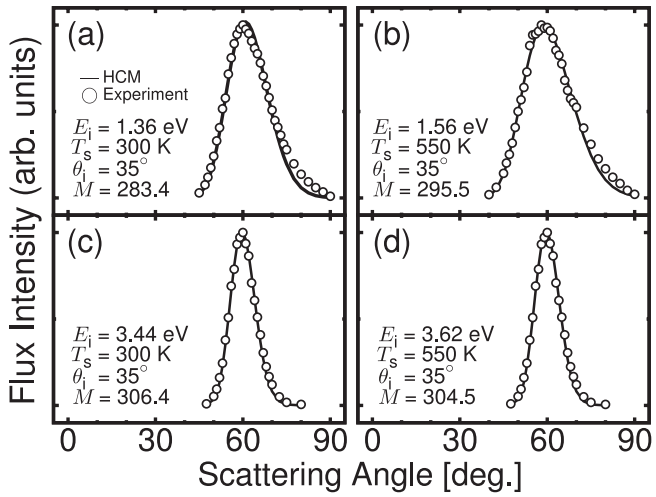

Fig. 4. Comparison of the observed angular flux distributions of the scattered Xe atoms with the best-fit theoretical curve of the simple Hard-Cube model. M is the mass of the model surface cube.

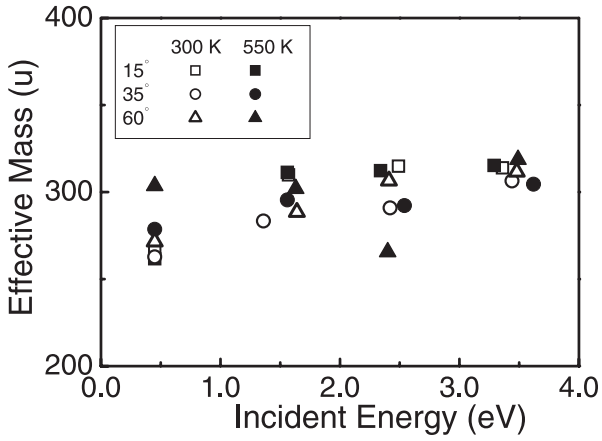

Fig. 5. The effective mass of the surface cube estimated from the angular flux distributions are plotted as a function of incidence energy for $\theta_i = 15°$, 35°, and 60° and $T_s = 300$ and 550 K.

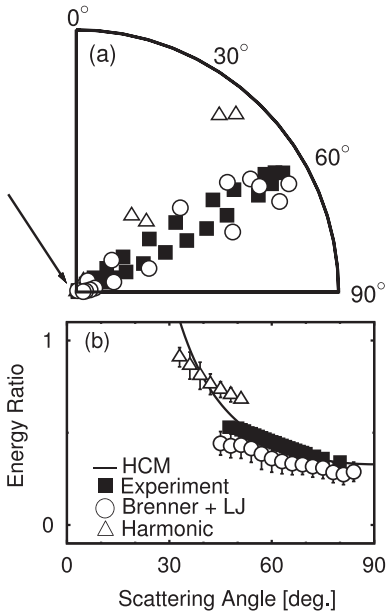

Fig. 6. (a) Angular distributions of the scattered Xe flux intensities, and (b) those of the energy ratios E_f/E_i from the experiment (■) and MD calculations using the two model potentials, the Brenner-LJ potential (○) and the harmonic model potential (△). ($E_i = 3.62$ eV, $T_s = 550$ K).

velocities, since the parallel momentum is conserved upon collision. The spread of the angular flux distribution is determined by the surface temperature. When the surface temperature is high, the velocity distribution of the cube becomes broader and the surface cube vibration has a greater influence on the scattered flux distribution. With increasing E_i the narrowing of the angular distribution also reflects the Hard-Cube model prediction. From these results we see that (i) thermal vibration of surface atoms has a pronounced effect upon the angular profiles of the scattered atoms, and (ii) with increasing the incidence energy the effect of the thermal vibration of the surface cube decreases.

In the Hard-Cube model the effective mass of the surface cube determines the energy transferred in the collision [28,29]. The effective mass of the surface cube M is determined from equation (3) by fitting to the angular flux distribution as shown in Figure 4. The result is plotted as a function of incidence energy for $T_s = 300$ K and 550 K in Figure 5. Notice that the effective surface mass is substantially constant for all incidence conditions and converges to approximately 310 u with increasing E_i. This means that Xe atoms undergo collisions with a cube composed of about 26 carbon atoms, regardless of the incidence angle, the incidence energy, and the surface temperature. The experimental results obtained for Xe-graphite (0001) surface scattering can be explained in terms of the simple Hard-Cube model in which an assembly of approximately 26 C atoms making up-and-down motions behaves like a hard cube. The collision of a Xe atom with a stationary cube with a mass of 310 u gives rise to the transfer of 80% of normal translational energy to the surface cube. The degree of normal translational energy transfer is dependent on only the ratio of the atomic Xe mass to the effective mass of graphite surface and not on the incidence angle nor incidence energy.

3.2 Molecular dynamics simulation

The molecular dynamics (MD) method was used to simulate the collisions of Xe with a graphite surface and to probe interaction potential which represents the graphite structure. We have simulated Xe atoms-graphite (0001) surface scattering using two model potentials for graphite; the harmonic model and the LJ potential model. Figure 6 shows the results: the polar plots of the angular flux distribution and the energy ratios E_f/E_i for $E_i = 3.62$ eV, $T_s = 550$ K, and $\theta_i = 35°$. In Figure 6a, the scattered flux distribution obtained with the harmonic model has a peak around the specular angle and the width of the

distribution is narrow. The harmonic model does not reproduce the experimental data and little energy transfer occurs, as shown in Figure 6b. On the contrary using the LJ potential model with the Brenner potential and the LJ potential, both the energy ratios and the flux distributions agree well with the experimental results. Thus the LJ potential model is considered to be appropriate for the scattering of Xe from the graphite (0001) surface. The potential of graphite is important for energy exchange on the collision.

4 Discussion

In general, angle-dependent energy ratios of E_f/E_i provide information on the interaction potential energy surface since the inelastically scattered particles probe the corrugation of the surface potential. As shown in Figure 3, the angle-dependent E_f/E_i ratios of Xe atoms scattered from a graphite (0001) surface have demonstrated the parallel momentum conservation even at hyperthermal incidence energies. The graphite surface acts as a flat surface during Xe atom collision. The experimental results can be interpreted fairly well in terms of the simple Hard-Cube model for a wide range of incidence conditions. The effective mass of the surface cube, which has been derived from the angular flux distribution in Figure 4, is found to be constant at 310 u, even when the incidence angle, the incidence energy, and the surface temperature are varied. Using the effective mass of the graphite surface in the simple Hard-Cube model, we have been able to estimate the energy transfers in the collision of a Xe atom with a graphite surface.

MD calculations have been carried out to simulate the collision dynamics and to probe the graphite potential. It has been found that the model potential employing the Brenner potential for the intraplaner C atoms and the LJ potentials for interplaner C–C interactions well reproduces the experiment. Particularly, the weak interplaner potential of graphite is essential in predicting the sufficient energy transfer. MD calculations enable us to visualize the motions of atoms involved in the scattering process. Figure 7 illustrates a snapshot of a Xe-graphite surface collision obtained from MD simulations using the LJ potential model for $E_i = 3.62$ eV, $T_s = 550$ K and $\theta_i = 35°$. As Xe approaches a graphite surface it widely pushes down the adjacent C atoms on the topmost graphite sheet and induces deformation. The deformation gives rise to slight elongation of C–C distances, deformation of the benzene rings, and decrease in interlayer atomic distances, and thus the deformations are induced in the lower sheets with time. Although the experimental results can be interpreted using a simple collision model comprising of a sphere and a cube (Hard-Cube model), in fact a lot of surface C atoms are involved in the collision and the dynamics of the scattering process are very complicated.

In Xe-graphite system, Xe (131 u) is much heavier than C (12 u). C atoms in the same graphite sheet are bound with each other with strong chemical bonds and the van der Waals radius of Xe (218 pm) is larger than

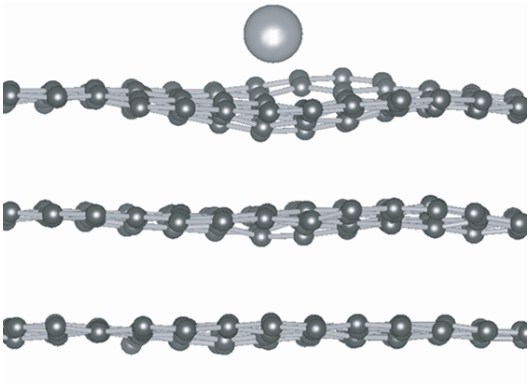

Fig. 7. A snapshot of a Xe atom collision with graphite (0001) surface from MD simulation for $E_i = 3.5$ eV, $\theta_i = 15°$, and $T_s = 550$ K.

the C–C bond distance (142 pm). Moreover since the interlayer interaction is weak but the intralayer interaction is very strong, the deformation is dispersed over the wide range of a whole topmost graphite sheet and makes the strain energy of the graphite dispersed. As a result, Xe pushes down the C atoms in the topmost graphite sheet and cannot penetrate deeply into the repulsive part of the interaction potential between Xe and an individual C on the surface. When the Xe atom collides with carbon atoms vibrating with thermal energies during the encounter, the impact exerted upon Xe from an individual C atom is small. Therefore Xe is scattered from an effectively flat potential surface of graphite, without feeling the structure corrugation due to individual C atoms, even at hyperthermal incidence energies, and thus the parallel momentum of the incident Xe atom is conserved. These motions of graphite sheets result in the fact that the simple Hard-Cube model well explains the experiment. The Hard-Cube model would be very useful in modeling the scattering dynamics of a heavy atom from a surface with a layer-structure material.

When a heavy atom impinges upon a surface at high collision energies, lattice deformation and thus dynamic corrugation in the gas-surface potential are induced. Ellison and Zare have observed an appreciable deviation from the PMC predictions of the angle-dependent ratios in Xe–Ni(111) scattering for a low incidence angle $\theta_i = 20°$ [17]. They interpret the results in terms of the lattice deformation upon Xe atom impact. In Xe-graphite (0001) scattering the topmost graphite sheet is pushed down by Xe collision and deformations of surface lattice are induced. In Figure 3 we see that the energy ratios for $\theta_i = 15°$ deviate from the PMC predictions probably due to the dynamic corrugation. Even though the interlayer potential disperses the deformation, as the incidence angle becomes upright and the perpendicular component of translational energy increases the dynamic corrugation is induced locally and Xe feels local dynamic corrugation. As the incidence angle becomes tilted, the perpendicular component of translational energy decreases and thus Xe feels less corrugation than for $\theta_i = 15°$. Therefore at

$\theta_i = 35°$ and 60° the energy ratios in Figure 3 agree with the PMC predictions better than for $\theta_i = 15°$.

In a rare gas scattering from a clean metal surface, the direct inelastic scattering process, in general, exhibits the angular distribution around the specular angle and little energy transfer between the gas and the surface. The harmonic model, which employs harmonic oscillator potential for the nearest neighbor surface atom interaction, well reproduces the observed scattering results from a metal surface and dynamics of energy transfer [19]. In Xe-graphite (0001) scattering, however, Xe is scattered at larger angles than the specular angle, and 80% of normal translational energy is transferred to the surface. Moreover, the relative amount of the normal translational energy transfer does not vary with incidence conditions. The experimental results are represented well by the simulation using the LJ potential model. Since graphite has a layer-structure and graphite sheets are bound with each other via a weak van der Waals interaction, large amplitude movements of carbon atoms in the topmost graphite sheet are induced by the incident Xe atom and help to transfer the translational energy of the incident atom to graphite vibrational energy via interlayer potential and to dissipate the energy. The cushion effect of the layer-structure in the collision is the special characteristics of graphite. In the Xe scattering from the graphite (0001) surface, the energy transfer is probably governed not by the incidence conditions but by the graphite surface properties.

5 Conclusion

The scattering of hyperthermal Xe from the graphite (0001) surface has been studied using a molecular beam-surface scattering technique and molecular dynamics calculations. The angular and velocity distributions of scattered Xe atoms have been measured under various incident beam conditions and at surface temperatures.

The ion lens system of the mass spectrometer detector was modified so that the ions formed by the electron bombardment ionizer of hyperthermal Xe atoms are repelled and detected efficiently. The TOF spectra observed exhibit sharp velocity distribution with only one velocity component, which is ascribed to the direct inelastic scattering process. The results of the angle-resolved energy ratios of the mean final translational energy over the mean incidence energy E_f/E_i agree well with those predicted from the conservation of the momentum parallel to the surface. The simple Hard-Cube model was applied to fit all of the observed angular distribution data to the theoretical distributions. We find that the theory predicts well for various incident beam and surface temperature conditions. Therefore we conclude that the scattering data can be explained in terms of the Hard Cube model. The effective mass of the surface cube is found to converge to approximately 310 u.

Molecular dynamics calculations have been conducted to simulate the scattering experiments. We have employed the interaction potential model to represent the Xe-graphite system that is the sum of the Brenner potential for intralayer carbon atoms and two Lennard-Jones potentials for Xe-graphite and interlayer C–C pair interaction. The potential model reproduces the layer-structure graphite and the dynamics of the energy transfer in the collision of a hyperthermal Xe atom with a graphite (0001) surface. The interlayer potential of graphite helps to dissipate the energy during collision.

References

1. M.H. Gordon, J.C. Tully, C.T. Rettner, C.B. Mullins, D.J. Auerbach, J. Chem. Phys. **94**, 1516 (1991)
2. J.A. Barker, C.T. Rettner, D.S. Bethune, Chem. Phys. Lett. **188**, 471 (1992)
3. R.J.W.E. Lahaye, A.W. Kleyn, S. Stole, S. Holloway, Surf. Sci. **338**, 169 (1995)
4. J. Harris, A.C. Luntz, J. Chem. Phys. **91**, 6421 (1989)
5. C.T. Rettner, D.S. Bethune, D.J. Auerbach, J. Chem. Phys. **91**, 1942 (1989)
6. Y. Teraoka, I. Nishiyama, Appl. Phys. Lett. **63**, 3355 (1993)
7. S.R. Leone, Jpn J. Appl. Phys. **34**, 2073 (1995)
8. F.O. Goodman, J. Phys. Chem. Solids **26**, 85 (1965)
9. R.M. Logan, R.E. Stickney, J. Chem. Phys. **44**, 195 (1966)
10. R.M. Logan, J.C. Keck, R.E. Stickney, Rarefied Gas Dynamics 4th Symposium **5**, 49 (1967)
11. C.T. Rettner, J.A. Barker, D.S. Bethune, Phys. Rev. Lett. **67**, 2183 (1991)
12. A. Raukema, R.J. Dirksen, A.W. Kleyn, J. Chem. Phys. **103**, 6217 (1995)
13. A. Amirav, M.J. Cardillo, P.L. Trevor, C. Lim, J.C. Tully, J. Chem. Phys. **87**, 1796 (1987)
14. J.C. Tully, J. Chem. Phys. **92**, 680 (1990)
15. D. Kulginov, M. Persson, C.T. Rettner, J. Chem. Phys. **106**, 3370 (1997)
16. A.F. Carlsson, R.J. Madix, Surf. Sci. **470**, 62 (2000)
17. M.D. Ellison, C.M. Matthews, R.N. Zare, J. Chem. Phys. **112**, 1975 (2000)
18. C.L. Kao, A. Carlsson, R.J. Madix, Surf. Sci. **565**, 70 (2004)
19. J.A. Barker, C.T. Rettner, J. Chem. Phys. **97**, 5844 (1992)
20. K. Shobatake, K. Ito, H. Yoshikawa, T. Ogi, H. Ariga, H. Ohashi, T. Fujimoto, Springer Ser. Solid-State Sci. **121**, 112 (1996)
21. M.B. Någård, P.U. Andersson, N. Marković, J.B.C. Pettersson, J. Chem. Phys. **109**, 10339 (1998)
22. Y. Watanabe, H. Yamaguchi, M. Hashinokuchi, K. Sawabe, S. Maruyama, Y. Matsumoto, K. Shobatake, Chem. Phys. Lett. **413**, 331 (2005)
23. H. Yoshikawa, H. Ohashi, K. Tabayashi, M. Suzui, T. Horigome, K. Hayakawa, S. Kato, K. Shobatake, Rev. Sci. Instrum. **70**, 1806 (1999)
24. Y. Matsumoto, N. Yamanishi, K. Shobatake, Journal Proc. 19th Int. Symp. Rarefied Gas Dynamics, 995 (1995)
25. N. Yamanishi, Y. Matsumoto, K. Shobatake, Phys. Fluids **11**, 3540 (1999)
26. L.K. Cohen, J. Chem. Phys. **99**, 9652 (1993)
27. D.W. Brenner, Phys. Rev. B **42**, 9458 (1990)
28. D. Velic, R.J. Levis, Chem. Phys. Lett. **269**, 59 (1997)
29. E.K. Grimmelmann, J.C. Tully, M.J. Cardillo, J. Chem. Phys. **72**, 1039 (1980)